

Recovering Power Factor Control Settings of Solar PV Inverters from Net Load Data

Samuel Talkington, Santiago Grijalva
School of Electrical and Computer Engineering
Georgia Institute of Technology
Atlanta, USA
{talkington,sgrijalva6}@gatech.edu

Matthew J. Reno, Joseph Azzolini
Electric Power Systems Research
Sandia National Laboratories
Albuquerque, USA
{mjreno,jazzoli}@sandia.gov

Abstract—Advanced solar PV inverter control settings may not be reported to utilities or may be changed without notice. This paper develops an estimation method for determining a fixed power factor control setting of a behind-the-meter (BTM) solar PV smart inverter. The estimation is achieved using linear regression methods with historical net load advanced metering infrastructure (AMI) data. Notably, the BTM PV power factor setting may be unknown or uncertain to a distribution engineer, and cannot be trivially estimated from the historical AMI data due to the influence of the native load on the measurements. To solve this, we use a simple percentile-based approach for filtering the measurements. A physics-based linear sensitivity model is then used to determine the fixed power factor control setting from the sensitivity in the complex power plane. This sensitivity parameter characterizes the control setting hidden in the aggregate data. We compare several loss functions, and verify the models developed by conducting experiments on 250 datasets based on real smart meter data. The data are augmented with synthetic quasi-static-timeseries (QSTS) simulations of BTM PV that simulate utility-observed aggregate measurements at the load. The simulations demonstrate the reactive power sensitivity of a BTM PV smart inverter can be recovered efficiently from the net load data after applying the filtering approach.

Index Terms—net load reactive power disaggregation, voltage regulation, reactive power control, advanced inverters, data-driven engineering

I. INTRODUCTION

The rapidly decreasing cost [1] of solar photovoltaics (PV) and other converter-based resources has prompted the introduction of advanced inverter control modes of varying popularity and deployment. In particular, reactive power control modes have become attractive for voltage regulation to counteract the inherent volatility of active power injections of distributed PV. This family of control modes have received significant attention in both industry and academia due to the

This work has been partially supported by the U.S. Department of Energy’s Office of Energy Efficiency and Renewable Energy (EERE) under Solar Energy Technologies Office (SETO) Agreement Number 34226. Sandia National Laboratories is a multi-mission laboratory managed and operated by National Technology and Engineering Solutions of Sandia, LLC., a wholly owned subsidiary of Honeywell International, Inc., for the U.S. Department of Energy’s National Nuclear Security Administration under contract DE-NA0003525. This paper describes objective technical results and analysis. Any subjective views or opinions that might be expressed in the paper do not necessarily represent the views of the U.S. Department of Energy or the United States Government.

reactive power priority specification of the IEEE 1547-2018 standard [2] on smart inverters.

Notably, many PV systems are not metered individually, which makes it difficult to know the precise active and reactive power injection values of BTM PV. Presently, distribution planners and operators have a need to ascertain the power factor control setting of BTM PV for correct operation of the grid. However, this setting may have never been reported upon installation; or may change without notice.

II. BACKGROUND

The simplest and most common advanced inverter control mode is the fixed power factor mode. In this mode the inverter controller is driven to inject or absorb reactive power such that a constant power factor setting is maintained at the PV injection point at all times. To achieve this control objective, the inverter reactive power output is set to be proportional to the PV real power output at every time step. This constant fixed power factor is referred to as the “control setting” or the “power factor setting”. Because the injection of active power from the PV system may cause overvoltages [3], lagging power factor settings are typically used to prevent these overvoltage conditions, i.e.:

$$\cos(\phi_V - \phi_I) < 0 \quad (1)$$

where ϕ_V , ϕ_I are the phase shifts in degrees of the PV line voltage and current, respectively.

The advantage of this control mode is primarily that of its simplicity. By default, IEEE 1547-2018 specifies a unity power factor for the fixed power factor control mode [2], thus not allowing for any generator voltage impact mitigation [4], [5].

A. Advanced Metering Infrastructure (AMI) Data

In this paper we consider the following net load advanced metering infrastructure (AMI) data stream:

$$\mathcal{D}_l = \{\mathbf{X}_t\}_{t=1}^M = \{(v_t^{pcc}, p_t^{net}, q_t^{net})\}_{t=1}^M \quad (2)$$

At timestep t in the dataset (2), v_t^{pcc} is the voltage magnitude measurement at the point of common coupling (PCC), and p_t^{net} , q_t^{net} are the net load active and reactive power measurements. The net power measurements are the additive combination of the native load demand and the PV generation.

We simulate this by adding together real, 15-minute granularity timeseries smart meter data for customers without BTM PV and yearlong 15-minute real power measurements from residential PV systems where PV reactive power is calculated based on the power factor. We assume that the sign convention for the PV power contributions is already applied, i.e., that injections are negative, and absorptions are positive. Therefore, the net AMI measurements are considered as:

$$\begin{aligned} p_t^{net} &= p_t^{pv} + p_t^{nat} \\ q_t^{net} &= q_t^{pv} + q_t^{nat} \end{aligned} \quad (3)$$

Note that a PV system with nonunity power factor control has *VAR-priority*, i.e., the real power generated by the PV system is curtailed when the inverter is operating at full capacity.

B. Parameterized Fixed Power Factor Control

The results of this paper hinge on a linear regression method to characterize the control behavior of a smart inverter operating in the fixed power factor mode. While operating in this mode, each PV system's reactive power response q_t^{pv} can be represented entirely by a single slope parameter $m = \frac{\Delta q}{\Delta p}$, which is known as the PV system's *sensitivity* of reactive power injections to real power injections. This sensitivity differs from voltage magnitude sensitivities, which have shown good success in estimating other BTM PV parameters [6]–[8]. If we had perfect access to the PV system's disaggregated real power measurements, we could reconstruct [9] the PV system's reactive power measurements as:

$$q_t^{pv} = m p_t^{pv} = \frac{\Delta q}{\Delta p} p_t^{pv} \quad (4)$$

This sensitivity defines a simple line in the complex power plane, which maintains $\cos(\phi_V - \phi_I)$ for any value of p_t^{pv} . The power factor setting pf can then be readily recovered using the common definition of the power factor $\cos(\phi_V - \phi_I)$:

$$\text{pf} = \cos(\phi_V - \phi_I) \implies \text{pf} = \cos\left(\arctan\left(\frac{\Delta q}{\Delta p}\right)\right) \quad (5)$$

Additionally, the setting can be recovered with a known PV apparent power measurement s_t^{pv} :

$$\text{pf} = \frac{p_t^{pv}}{\|s_t^{pv}\|_2} \implies \text{pf} = \frac{q_t^{pv}}{\frac{\Delta q}{\Delta p} \|s_t^{pv}\|_2} = \frac{q_t^{pv}}{m \|s_t^{pv}\|_2} \quad (6)$$

Note that for the typical lagging power factor case, the sensitivity is less than or equal to zero, and the complex power line is fixed at the origin.

III. FILTERING NET LOAD AMI DATA

The AMI data contain contributions from both the native reactive power demand and the reactive power absorbed or injected by the PV smart inverter. Therefore, it is necessary to filter the net load AMI measurements in order to more accurately approximate the power factor control of the PV by itself.

Algorithm 1: Net Load Data Filter

Result: A subset \mathcal{D}_l^δ of historical AMI dataset \mathcal{D}_l that exposes the approximate behavior of the fixed power factor control curve.

load dataset \mathcal{D}_l ;

initialize $\mathcal{D}_l^\delta = \{\mathbf{X}_t \in \mathcal{D}_l : p_t^{net} < 0\}$;

remove nighttime measurements in \mathcal{D}_δ compute V_δ ;

compute \hat{S}_{rated} ;

for \mathbf{X}_t **in** \mathcal{D}_l **do**

if $v_t > V_\delta$ **then**

if $s_t^{net} > \hat{S}_{rated}$ **then**

 append \mathbf{X}_t to \mathcal{D}_δ ;

else

 continue;

end

else

 continue;

end

end

A. Extreme Value Filter

Visualization techniques such as those shown in Figures 1 and 2 reveal that historical measurements with abnormally high voltage magnitude measurements closely approximate the true control curve. Therefore, we propose the use of a percentile-based filtering method to help expose the control sensitivity. This is done by computing percentile values for all historical voltage measurements at the load. We then form the filtered dataset \mathcal{D}_l^δ with M' samples from the original dataset \mathcal{D}_l by selecting a cutoff percentile value V_δ :

$$\mathcal{D}_l^\delta = \{\mathbf{X}_t \in \mathcal{D}_l : v_t^{pcc} > V_\delta\} \quad (7)$$

The experiments in this paper are conducted with AMI datasets where the BTM PV have relatively high power factors, 0.9 to 1.0 power factor. In extreme scenarios where the power factor control setting of the PV system is set to lower values, for example, $\text{pf} = 0.6$, the excess reactive power absorption during PV production would cause the extreme *undervoltages* to best approximate the curve.

For the remainder of the paper, we will denote the filtered observations as vectors with the symbol $\tilde{\cdot}$, and drop the subscript l . Specifically, $\{(\tilde{v}_t, \tilde{p}_t, \tilde{q}_t)\}_{t=1}^{M'} = (\tilde{\mathbf{p}}, \tilde{\mathbf{q}}, \tilde{\mathbf{v}})$.

In Algorithm 1, we show our heuristic for finding the filtered dataset \mathcal{D}_l^δ from the full historical AMI dataset \mathcal{D}_l that exposes the approximate behavior of the fixed power factor control curve. This is done by considering observations that occur during δ th-percentile extreme overvoltage events.

Experimentally, we have found that observations in the 90th–99th percentile of historical voltage measurements are often due primarily to be PV injections.

B. Observations Near Rated PV Size

Note that if the PV apparent power s_t^{pv} is close to the rated value of the PV, the fixed power factor control response

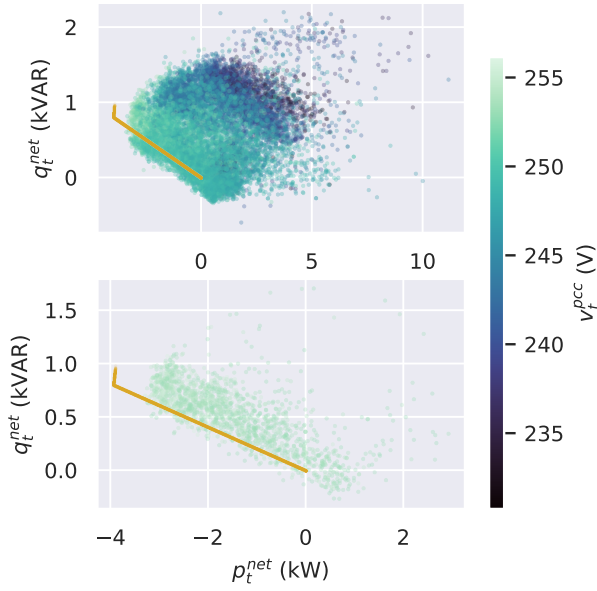


Figure 1. Top: example of a typical scatterplot for a load with BTM PV operating under fixed nonunity power factor. Each point represents a net load reactive power and net load real power measurement from a 1 year, 15 minute sampling interval AMI dataset. Bottom: the same dataset filtered with respect to extreme overvoltages with a cutoff value of $\delta = 0.99$. The actual PV measurements are shown in orange.

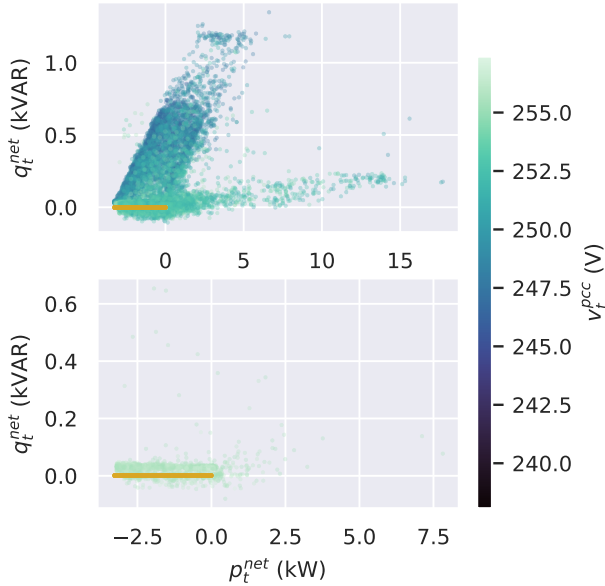


Figure 2. Top: example of a typical scatterplot for a load with BTM PV operating under unity power factor. Bottom: the same dataset filtered with respect to extreme overvoltages with a cutoff value of $\delta = 0.99$. The actual PV measurements are shown in orange.

becomes nonlinear as shown in Figs. 1 and 2. However, the linearization of the control curve remains accurate for values inside the inverter capability curve [10].

To avoid the nonlinear region, we incorporate an additional filtering step that discards measurements with net apparent

power that are close to a fraction of the expected PV size \hat{S}_{rated} that is set by the user. For the purpose of this paper, we take up to the 80th percentile of apparent power measurements.

C. Constant Reactive Power Offset

Note that after applying the filtering Algorithm 1, the points may closely follow the correct reactive power sensitivity, but may still contain a constant reactive power offset in the complex power plane.

To counteract this, we form a modified parameter vector as follows:

$$\Theta = \begin{bmatrix} \frac{\Delta q}{\Delta p} & b \end{bmatrix}^T \quad (8)$$

Where b is the y-axis offset in the complex power plane. Similarly, we append a column of ones to the data matrix as follows:

$$\mathbf{A} = \begin{bmatrix} \vdots & \vdots \\ \tilde{\mathbf{p}} & 1 \\ \vdots & \vdots \end{bmatrix} \quad (9)$$

The PV reactive power approximation model is then simply a line in slope-intercept form $y = mx + b$, and can be written as $\hat{\mathbf{q}}^{pv} = \mathbf{A}\Theta$. Note that the PV reactive power timeseries can be approximately disaggregated from the net load measurements during the filtered measurement time points:

$$\hat{\mathbf{q}}^{pv} = \mathbf{A}\Theta = \frac{\Delta q}{\Delta p} \tilde{\mathbf{p}} + b \approx \tilde{\mathbf{q}}^{pv} \quad (10)$$

IV. FIXED POWER FACTOR ESTIMATION

After filtering, the load AMI dataset (7) observations are primarily composed of the PV contribution in (3), i.e. $|p_t^{pv}| > |p_t^{nat}|$ and $|q_t^{pv}| > |q_t^{nat}|$, and we assume that the native contribution can be treated as noise.

Applying equations (4) and (5) allows us to treat the estimation of the power factor control setting as a linear regression problem. Then, by using (5), the power factor control parameter can be recovered entirely through the slope of the line in the complex power plane (the sensitivity) that best fits the filtered data. In this section, we will discuss different ways to find the best slope.

A. The Least Squares Solution

A straightforward method to recover the exposed sensitivity is to apply ordinary least squares regression. Using the filtered real and reactive power timeseries vectors $\tilde{\mathbf{p}}$ and $\tilde{\mathbf{q}}$, the power factor control setting can be recovered by finding the slope and intercept in the complex power plane that minimizes the sum of squares of the residuals:

$$\text{minimize}_{\Theta} \|\tilde{\mathbf{q}} - \mathbf{A}\Theta\|_2^2 \quad (11)$$

Which is known to have a unique closed form solution [11]:

$$(\mathbf{A}^T \mathbf{A})^{-1} \mathbf{A}^T \tilde{\mathbf{q}} \quad (12)$$

B. Building Robustness to Outliers

While the least squares regression problem (11) and its solution (12) is sufficient for many practical scenarios with the filtering methods that we have outlined, the squared loss function is overly sensitive to outliers. Because the filtering method is empirical, the impact of the native reactive power demand \tilde{Q}_t on the measurements Q_t^{net} may be significant in practice and may skew or corrupt the true sensitivity hidden behind the net observations. To address this issue, we develop robust linear regression models in this section through the use of several common loss functions.

1) ℓ_1 Norm Approximation: Experimentally, we have observed that the noise after pre-processing is often “sparse” in that there are very few outlier observations in comparison with the overall power factor trend line after filtering to expose the sensitivity.

In these scenarios, it is common [12] to set the regression loss function to be the ℓ_1 norm of the residuals, also known as the “absolute loss”:

$$\underset{\Theta}{\text{minimize}} \|\tilde{\mathbf{q}} - \mathbf{A}\Theta\|_{\ell_1} \quad (13)$$

where the loss function in (13) is the sum of the absolute value of the residuals:

$$\|\tilde{\mathbf{q}} - \mathbf{A}\Theta\|_{\ell_1} = \sum_{t=1}^{M'} |\tilde{q}_t - a_t^T \Theta| \quad (14)$$

2) *Huber Loss Function*: The user can trade-off between the higher variance in (12) and higher bias in (13) by using the model below in (15), which utilizes the Huber loss function. This is a statistical tool for reducing the sensitivity of a model to outliers, typically defined as:

$$\underset{\Theta}{\text{minimize}} l_\epsilon(\tilde{\mathbf{q}}, f(\Theta)) \quad (15)$$

Where the Huber loss $l_\epsilon(\tilde{\mathbf{q}}, f(\Theta))$ is defined [11], [12] as:

$$l_\epsilon = \begin{cases} \|\tilde{\mathbf{q}} - \mathbf{A}\Theta\|_2^2 & \|\tilde{\mathbf{q}} - \mathbf{A}\Theta\|_2 \leq \epsilon \\ \epsilon(\|\tilde{\mathbf{q}} - \mathbf{A}\Theta\|_{\ell_1} - \frac{1}{2}\epsilon) & \text{otherwise} \end{cases} \quad (16)$$

The loss function (16) is identical to the squared loss in (11) for absolute errors less than ϵ , and is a linear function for errors greater than ϵ . Note that as $\epsilon \rightarrow 0$, the Huber loss function becomes similar to ℓ_1 norm approximation loss function in (13). The error threshold value ϵ is set by the user. Figure 3 shows the tradeoff curves for this parameter and Section V describes the result.

V. EXPERIMENTAL RESULTS AND PERFORMANCE

Using quasi-static timeseries (QSTS) simulation algorithms [3], [13], [14], we construct semi-synthetic historical AMI datasets to verify, test, and compare the models. The AMI load data used are actual native load active and reactive measurements from an electric utility. The PV real power injections are also measurements from actual residential PV systems at 15-minute granularity for a year. The actual PV

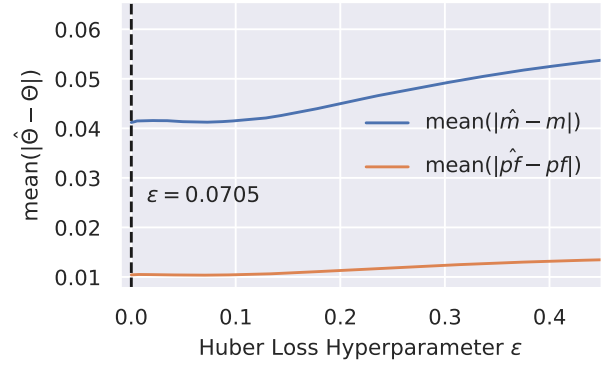


Figure 3. Estimation error tradeoff curves for the Huber regression loss function for many values of ϵ

systems were all installed with unity power factor, so for this experiment, the power factors of some of the PV systems were modified. 50 PV systems were modified to non-unity power factors between 0.9 and 0.99. The PV reactive power for these systems is calculated based on the measured real power and the assigned power factor. The net load for each customer is then the sum of the load and PV measurements. The resulting voltage is then determined from QSTS power flow solutions. For additional details on the load modeling used, we refer the reader to [13].

To evaluate the performance of the model, we use several error metrics. The first is the mean absolute error (MAE) of the sensitivity and power factor estimators for the L test loads:

$$\text{MAE}(\hat{x}) = \sum_{l=1}^L \frac{\|\hat{x}_l - x_l\|}{L} \quad (17)$$

Where \hat{x} is the estimated control parameter (either the sensitivity or power factor) and x is the true parameter.

The second is the mean squared-error (MSE) of the predicted daytime PV reactive power timeseries using the estimated sensitivity parameter. Note that there are two ways of evaluating this. The first is the “prescient” case, where we assume to have perfectly disaggregated the M true PV real power timeseries measurements p_t^{pv} , $t = 1, \dots, M$ from the net load AMI timeseries, which we then use to compute the estimated PV reactive power timeseries measurements \hat{q}_t^{pv} using (10).

$$\text{MSE}^{\text{prescient}}(\hat{\Theta}) = \frac{\sum_{t=1}^{M'} (\hat{m} p_t^{pv} - \hat{q}_t^{pv})^2}{M'} \quad (18)$$

The third is the root-mean-squared-deviation, which is in the same units of the estimated parameter (kVAR) [12]:

$$\text{RMSE}^{\text{prescient}}(\hat{\Theta}) = \sqrt{\frac{\sum_{t=1}^{M'} (\hat{m} p_t^{pv} - \hat{q}_t^{pv})^2}{M'}} \quad (19)$$

Note that these equations only use the estimated reactive power sensitivity, and do not use the constant reactive power offset term \hat{b} (the y-intercept).

Table I
PARAMETER ESTIMATION PERFORMANCE SUMMARY BY MEAN ABSOLUTE ERROR (MAE)

Type	Algorithm Objective			
	ℓ_1 Norm		Huber, $\epsilon = 7 \times 10^{-2}$	
	Sensitivity	PF	Sensitivity	PF
Unity	0.00341	0.0000571	0.00343	0.00343
Nonunity	0.0412	0.0104	0.0411	0.0103

Table II
 ℓ_1 MEAN MODEL PREDICTIVE PERFORMANCE SUMMARY, NONUNITY POWER FACTOR

Error Type	Evaluation Method	
	Prescient	Filtered
MSE	0.0195	0.0506
RMSE (kVAR)	0.0923	0.194

We will also evaluate the “filtered” or “disaggregated” error performance. By this we mean that we will *include* the reactive offset parameter (the Q -axis intercept), and use the full equation of the best-fitted line in the complex power plane as an estimate for the PV reactive power. The function is evaluated with the filtered real power timeseries values $\tilde{p}_t, t = 1, \dots, M'$. The higher kVAR deviation for the “disaggregated” calculation is due to the fact that the disaggregation itself has not been fully solved, in that $\tilde{\mathbf{p}}$ in (9) only *approximates* the true PV real power generation \mathbf{p}^{pv} that drives the control behavior in actuality, as described in (4).

$$\text{MSE}^{\text{filtered}}(\hat{\theta}) = \frac{\sum_{t=1}^{M'} (\hat{m}\tilde{p}_t^{pv} + \hat{b} - \tilde{q}_t^{pv})^2}{M'} \quad (20)$$

Similar to (19), we compute the RMSE for the filtered measurements as follows:

$$\text{RMSE}^{\text{filtered}}(\hat{\theta}) = \sqrt{\frac{\sum_{t=1}^{M'} (\hat{m}\tilde{p}_t^{pv} + \hat{b} - \tilde{q}_t^{pv})^2}{M'}} \quad (21)$$

The Huber regression loss parameter ϵ described in (16) is tuned empirically by solving the optimization problem in (15) for many values of epsilon using [15]. It is found that a value of $\epsilon \approx 7.05 \times 10^{-2}$ yields the best overall performance for the datasets we have studied. The tradeoff curves for this experiment are shown in Fig. 3.

In Figures 4 and 5, we depict the performance of the ℓ_1 norm approximation model in (13) for 50 loads with BTM PV with nonunity power factor control, and for 200 loads with unity power factor control.

Additionally, Table I shows the mean values of these errors, and also those of the Huber regression (15). The predictive performance for the reactive disaggregation using (18)-(21) is shown in Table II.

In Fig. 6, we show an example reactive power sensitivity fit for a dataset filtered with percentile cutoff parameter $\delta = 0.90$. The load contains BTM PV operating under fixed nonunity power factor. By filtering for the 90th percentile voltage observations, the reactive power sensitivity becomes exposed and can be easily estimated.

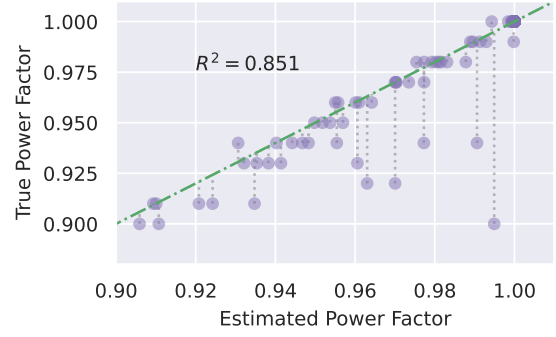


Figure 4. Scatterplot of estimated power factor vs. true power factor for all datasets studied.

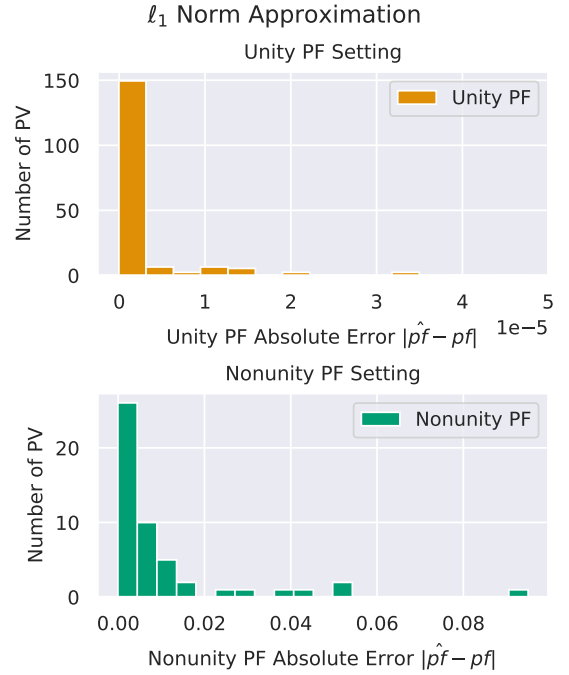


Figure 5. Top: histograms of power factor estimation mean absolute error (MAE) for 200 loads with unity power factor BTM PV. Bottom: mean absolute error (MAE) for 50 loads with nonunity power factor BTM PV.

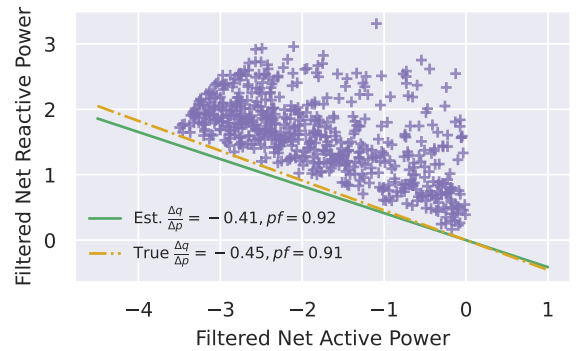


Figure 6. Example of an estimated nonunity power factor control curve (green), real PV measurements (orange), and a filtered dataset (purple).

VI. DISCUSSION

There are limitations to the method shown in this paper. Primarily, it is not trivial to disaggregate the net load reactive power measurements even if the slope is accurately estimated. This is because the PV reactive power is a function of the PV real power, meaning that the net load AMI measurements would have to be disaggregated *a priori* in order to construct the PV reactive power timeseries with the estimated sensitivity.

There are many opportunities for future work in improving and formalizing the filtering methodology. For instance, our empirical method for filtering with respect to the capability curve of the inverter can be improved with the use of a PV size estimation algorithm, such as the one in [16].

It may also be feasible to construct probabilistic filtering methods, or incorporate additional feeder model information to find the most salient observations. With these methods, the reactive power disaggregation can be improved. This also creates an opportunity for future work in ensuring that the methods can generalize to loads that have voltage regulating equipment.

VII. CONCLUSION

We have presented a linear sensitivity-based method for distribution engineers or utilities to determine a fixed power factor control setting from net load, aggregate AMI data. The linear regression methods and filtering approaches used to achieve the estimation are simple and interpretable, allowing for fast and efficient calculations in practice.

In summary, our methods indicate that it is possible to recover a PV system's power factor control setting with a mean absolute error of approximately 0.01 for nonunity power factor settings, and on the order of 1×10^{-4} for unity power factor settings.

REFERENCES

- [1] D. Feldman, V. Ramasamy, R. Fu, A. Ramdas, J. Desai, and R. Margolis, "U.S. Solar Photovoltaic System and Energy Storage Cost Benchmark: Q1 2020," NREL/TP-6A20-77324. [Online]. Available: <https://www.nrel.gov/docs/fy21osti/77324.pdf>
- [2] "IEEE Standard for Interconnection and Interoperability of Distributed Energy Resources with Associated Electric Power Systems Interfaces," *IEEE Std 1547-2018 (Revision of IEEE Std 1547-2003)*, pp. 1–138, 2018.
- [3] J. Seuss, M. J. Reno, R. J. Broderick, and S. Grijalva, "Analysis of PV Advanced Inverter Functions and Setpoints under Time Series Simulation," no. SAND2016–4856, 1259558, May 2016. [Online]. Available: <https://www.osti.gov/biblio/1259558>
- [4] R. O'Connell, C. Volkmann, and P. Brucke, "Regulating Voltage: Recommendations for Smart Inverters," 2019. [Online]. Available: <https://gridlab.org/publications>
- [5] R. J. Broderick, M. J. Reno, M. S. Lave, J. A. Azzolini, L. Blakely, J. Galtieri, B. Mather, A. Weekley, R. Hunsberger, M. Chamana, Q. Li, W. Zhang, A. Latif, X. Zhu, S. Grijalva, X. Zhang, J. Deboever, M. U. Qureshi, F. Therrien, J.-S. Lacroix, F. Li, M. Belletête, G. Hébert, D. Montenegro, and R. Dugan, "Rapid QSTS Simulations for High-Resolution Comprehensive Assessment of Distributed PV," 3 2021. [Online]. Available: <https://www.osti.gov/biblio/1773234>
- [6] S. Talkington, S. Grijalva, and M. J. Reno, "Power Factor Estimation of Distributed Energy Resources Using Voltage Magnitude Measurements," *Journal of Modern Power Systems and Clean Energy*, vol. 9, no. 4, pp. 859–869, 2021.

- [7] S. Grijalva, A. Khan, J. Sihno Mbeleg, C. Gomez-Peces, M. Reno, and L. Blakely, "Estimation of PV Location in Distribution Systems based on Voltage Sensitivities," in *2021 IEEE North American Power Symposium (NAPS)*, 04 2021.
- [8] C. Gomez-Peces, S. Grijalva, M. J. Reno, and L. Blakely, "Estimation of PV Location based on Voltage Sensitivities in Distribution Systems with Discrete Voltage Regulation Equipment," in *IEEE PowerTech Madrid*, 2021.
- [9] S. Karagiannopoulos, R. Dobbe, P. Aristidou, D. Callaway, and G. Hug, "Data-driven control design schemes in active distribution grids: Capabilities and challenges," in *2019 IEEE Milan PowerTech*, 2019, pp. 1–6.
- [10] J. McDowell, R. Walling, W. Peter, E. Von Engeln, E. Seymour, R. Nelson, L. Casey, A. Ellis, and C. Barker, "Reactive Power Interconnection Requirements for PV and Wind Plants," Tech. Rep. SAND2012-1098, 1039006, Feb. 2012. [Online]. Available: <http://www.osti.gov/servlets/purl/1039006/>
- [11] S. P. Boyd and L. Vandenberghe, *Convex Optimization*. Cambridge, UK ; New York: Cambridge University Press, 2004.
- [12] T. Hastie, R. Tibshirani, and J. Friedman, *The Elements of Statistical Learning: Data Mining, Inference, and Prediction*, 2nd ed. Springer Series in Statistics, Jan. 2017.
- [13] J. Peppanen, J. Deboever, M. Hernandez, and M. Rylander, "Enhanced Load Modeling: Study of Practical Load Modeling Methods on Distribution Feeders with Behind-The-Meter PV Systems," EPRI/3002018983, 06 2020. [Online]. Available: <https://www.epri.com/research/products/000000003002018983>
- [14] M. U. Qureshi, S. Grijalva, and M. J. Reno, "A fast quasi-static time series simulation method for pv smart inverters with var control using linear sensitivity model," in *2018 IEEE 7th World Conference on Photovoltaic Energy Conversion (WCPEC) (A Joint Conference of 45th IEEE PVSC, 28th PVSEC 34th EU PVSEC)*, 2018, pp. 1614–1619.
- [15] S. Diamond and S. Boyd, "CVXPY: A Python-embedded modeling language for convex optimization," *Journal of Machine Learning Research*, vol. 17, no. 83, pp. 1–5, 2016.
- [16] K. Mason, M. J. Reno, L. Blakely, S. Vejdan, and S. Grijalva, "A deep neural network approach for behind-the-meter residential PV size, tilt and azimuth estimation," *Solar Energy*, vol. 196, pp. 260–269, Jan. 2020.